Influence of swelling-degradation degree on rheological properties, thermal pyrolysis kinetics, and emission components of waste crumb rubber modified bitumen

Ren, S.; Liu, X.; Lin, P.; Erkens, S.

DOI
10.1016/j.conbuildmat.2022.127555

Publication date
2022

Document Version
Final published version

Published in
Construction and Building Materials

Citation (APA)
Ren, S., Liu, X., Lin, P., & Erkens, S. (2022). Influence of swelling-degradation degree on rheological properties, thermal pyrolysis kinetics, and emission components of waste crumb rubber modified bitumen. *Construction and Building Materials*, *337*(127555), 1-15. Article 127555. https://doi.org/10.1016/j.conbuildmat.2022.127555

Construction and Building Materials 337 (2022) 127555

Contents lists available at ScienceDirect

Construction and Building Materials

journal homepage: www.elsevier.com/locate/conbuildmat

Influence of swelling-degradation degree on rheological properties, thermal pyrolysis kinetics, and emission components of waste crumb rubber modified bitumen

Shisong Ren, Xueyan Liu, Peng Lin *, Sandra Erkens

Section of Pavement Engineering, Faculty of Civil Engineering & Geosciences, Delft University of Technology, Stevinweg 1, 2628 CN Delft, the Netherlands

ARTICLE INFO

Keywords:
Crumb rubber modified bitumen
Swelling-degradation behaviors
Rheological properties
Thermal pyrolysis kinetics
Volatile components

ABSTRACT

This study investigated the effects of swelling-degradation degree on the rheological properties and thermal pyrolysis behaviors of crumb rubber modified bitumen (CRMB). The equilibrium viscosity of CRMB in 160 °C-swelling process is 10.5 Pa·s at 8 h. During the 200°C-degradation procedure, the viscosity increased to a maximum value of 20.58 Pa·s at 7.5 h and gradually reduced to a stable value of 11.09 Pa·s after 35 h. The swelling and degradation processes exhibit the opposite influence on the rheological properties of CRMB. Moreover, the degradation process accelerated the pyrolysis rate of CRMB but hindered the release of toxic gas CO and hydrocarbons.

1. Introduction

From the viewpoint of sustainable pavement materials, the crumb rubber (CR) from waste tires is proposed as an available modifier of bitumen binder [1]. It has been proved that the utilization of CR powder was beneficial to improve the high-and-low temperature properties of bitumen and extend the service life of asphalt roads [2]. At the same time, rubber asphalt exhibits advantages in the reduction of traffic noise and pavement thickness. In addition, the carbon emissions reduction of rubber asphalt has been validated [3]. Therefore, the CRMB binder is attracting more attention from pavement researchers and engineers.

However, the CRMB technology is still facing lots of challenges regarding the insufficient performance, workability, and compatibility aspects. Generally, it is difficult for CRMB binders with low CR content to meet the requirements of sufficient rheo-mechanical performance. To enhance the rutting, cracking, and aging resistance performance of bitumen, large amounts of CR powders (more than 15 wt%) were incorporated into the bitumen matrix, which resulted in the high viscosity and worse workability of CRMB binder. Moreover, the dispersion degree of rubber particles in bitumen is weakened and the phase separation would occur easily during the thermal storage and transportation processes [4]. To address these issues, the compound modification technology was proposed by supplementing other polymer additives, such as waste polyethylene terephthalate (PET) [5] and styrene-butadienestyrene (SBS) [6]. In addition, to reduce the viscosity and improve the compatibility between CR and bitumen, the warm-mixed and bio-modified CRMB was developed by incorporating the warm mixing agents [7,8] and bio-based modifiers [9–11]. Some chemical procedures were also proposed to enhance the low-temperature cracking and compatibility of CRMB binder through the desulfurization, microwave, and surface activation methods [12–15]. However, it should be mentioned that the basic prerequisites for advanced method development of CRMB binder are to fully understand the interaction mechanism between the CR powders and bitumen matrix.

Experimental and numerical research has been conducted to explore the fundamental interaction between CR and bitumen, and the corresponding influence on the rheological and mechanical properties of CRMB binder. A consensus is reached that the swelling and degradation are mainly two reaction types during the mixing of CR and bitumen [16]. The rubber particles absorb the light-weight oily components in bitumen (saturate and aromatic fractions) together with its volume expansion, which is called the swelling process. Meanwhile, under the high-temperatures condition, the chemical bonds and polymer network structure in CR would be damaged, which leads to the release and dissolution of CR molecules into the bitumen matrix. According to the basic principle of swelling and degradation interaction, it is expected that the swelling and degradation degree significantly affect the rheological and aging behaviors of rubber bitumen. Li et al. validated that the

* Corresponding author.
E-mail addresses: Shisong.Ren@tudelft.nl (S. Ren), x.liu@tudelft.nl (X. Liu), p.lin-2@tudelft.nl (P. Lin), S.M.J.G.Erkens@tudelft.nl (S. Erkens).

https://doi.org/10.1016/j.conbuildmat.2022.127555
Received 11 February 2022; Received in revised form 1 April 2022; Accepted 15 April 2022
Available online 23 April 2022

Table 1
Conventional properties and chemical components of virgin bitumen.

Parameters	Value	Standard method
25 °C Penetration (0.1 mm)	67	ASTM D5
Softening point (°C)	48.4	ASTM D36
10 °C Ductility (cm)	85.2	ASTM D113
Saturates (S, wt%)	13.35	ASTM D4124
Aromatics (A, wt%)	17.35	
Resins (R, wt%)	39.70	
Asphaltenes (At, wt%)	29.60	
Colloidal index CI*	0.753	

* Colloidal index CI = (asphaltenes + saturates)/(aromatics + resins).

rubber adsorption hindered the oxygen attack and enhanced the aging resistance of bitumen [17]. Dong et al. [18] and Wang et al. [19] investigated the swelling behaviors of CRMB binders through experimental characterization and numerical simulation. It was suggested that the increasing swelling degree improved the softening point but deteriorated the low-temperature cracking resistance of the CRMB binder. Huang et al. [20] compared the components distribution and rheological properties of CRMB binders with different degradation degrees, and the results revealed that the high degradation degree was beneficial to improve the workability and storage stability but weaken the rutting resistance of rubber bitumen.

The special smell is another key limitation of CRMB, which is associated with the workers' health and air environment. The gaseous products during the mixing process of CR powder in bitumen are generated at high temperatures. However, the thermal degradation behaviors and volatiles components of the CRMB binder are still unclear. The TG-FTIR technology has been proved as an efficient method to study the thermal pyrolysis behavior and gaseous products of waste solid materials simultaneously, such as plastics [21], food waste [22], oil sand bitumen [23,24], natural rubber [25], and waste bicycle tire [26], etc. Meanwhile, the thermal degradation and pyrolysis products of bitumen also can be estimated by using the TG-FTIR method [27]. The combustion mechanism of the bitumen binder was investigated using TG-FTIR with an O_2/N_2 mixed gas environment and low heating rate [28–30]. The results showed that the released volatiles was mainly generated at 300–570 °C, and the main products during the bitumen pyrolysis process were CO_2, CO, H_2O, hydrocarbons, formaldehyde, aromatic compounds, etc. Hao et al. [23] also reported that the CO_2, CO, CH_4, light C^{2+} aliphatic hydrocarbons, and light aromatics were the typical gaseous products of oil sand bitumen. In addition, Elkashef et al. [31] employed TG-FTIR to assess the thermal stability and analyze the evolved gas of rejuvenated bitumen. It was revealed that the thermal stability of rejuvenated bitumen was similar to the aged binder, and the characteristic peaks of the rejuvenator could be used as an indication of the thermal degradation rate of rejuvenated bitumen.

From the literature review, it is clear that the swelling-degradation interaction significantly determines the rheological and mechanical properties of the CRMB binder. Meanwhile, the TG-FTIR method is an efficient way to explore the combustion mechanism and pyrolysis products distribution of bituminous materials. However, limited research focused on the continuous swelling-degradation behaviors of the CRMB, and the difference in rheological properties between CRMB binders with various swelling-degradation stages. In addition, the pyrolysis behaviors and gaseous products of CRMB binder considering the influence of swelling-degradation degree have not been studied yet. Therefore, this research aims to systematically explore the continuous swelling-degradation behaviors and monitor the rheological properties variation of the CRMB during the continuous swelling-degradation processes for the first time, together with the preliminary study on the combustion and pyrolysis behaviors of CRMB binder with the influence of swelling-degradation degree. The outcomes from this study will guide the preparation and application of the CRMB binder with various swelling-degradation levels to some extent.

Table 2
The physical properties of crumb rubber powder.

Physical properties		Particle size distribution	
Parameters	Value	Mesh	Percentage (wt%)
Density (g.cm^{-3})	1.20	30–40	34.35
Moisture content (wt%)	0.30	40–50	22.52
Ash content (wt%)	5.40	50–60	7.34
Mental content (wt%)	0.006	60–70	14.24
Rubber hydrocarbon (wt%)	55.8	70–80	2.79
Carbon content (wt%)	30.2	80–90	6.54
Acetone extract (wt%)	10.7	greater than90	12.24

2. Materials and research methodologies

2.1. Raw materials

The Marui crude oil-based virgin bitumen with a penetration grade of 60–80 was utilized in this study. The physical indices (Penetration, softening point, and ductility) and chemical components distribution (saturates S, aromatics A, resins R, and asphaltenes A_s) are listed in Table 1. The virgin bitumen and crumb rubber powder utilized in this study are commonly-used in Jiangsu Province, China, and are consistence with our previous studies [15,19]. Both the virgin bitumen and crumb rubber are provided by Jiangsu Tiannuo Company Ltd. The CR modifier with particle sizes ranging from 0 to 0.600 mm came from the ambient grinding process of scrap truck tires, and its basic properties are displayed in Table 2. In addition, the particle size distribution of CR powders after the sieving procedure is also shown in Table 2.

2.2. Research methodologies

It is difficult to separate the swelling and degradation reactions of the CRMB binder. From the previous studies [18,19], the reaction temperatures for swelling and degradation processes were selected as 160 and 200 °C, respectively. The research methodologies for this study are illustrated in Fig. 1, and elaborated as follows:

- The CR powders with particle sizes ranging from 0 to 0.600 mm and mass fraction of 20 % were incorporated into the heated bitumen at 160 °C. The rotating speed of the blender was 1000 rpm, and the swelling time was recorded.
- The mixed CRMB specimen was taken out per 1 h through a clean sample spoon carefully to monitor the viscosity variation of the CRMB binder during the swelling process with the rotational viscometer (RV).
- When the viscosity value was kept constant, the system temperature rose from 160 to 200 °C directly to perform the degradation process. Moreover, the rotating speed during the degradation process was the same as that in the swelling procedure (1000 rpm).
- After the temperature reached 200 °C, the degradation time was recorded and the viscosity of CRMB binder during the degradation process was measured per 2.5 h.
- Meanwhile, the CRMB samples with different swelling and degradation degrees were collected and subjected to the dynamic shear rheometer (DSR) test to investigate the rheological and mechanical properties that vary as a function of swelling and degradation durations.
- Furthermore, the thermal pyrolysis characteristics and volatile components of CRMB binders with different swelling-degradation degrees were investigated through the TG-FTIR method.

2.3. Experimental tests

2.3.1. RV and DSR tests

In this study, the Brookfield DV rotational viscometer (RV,

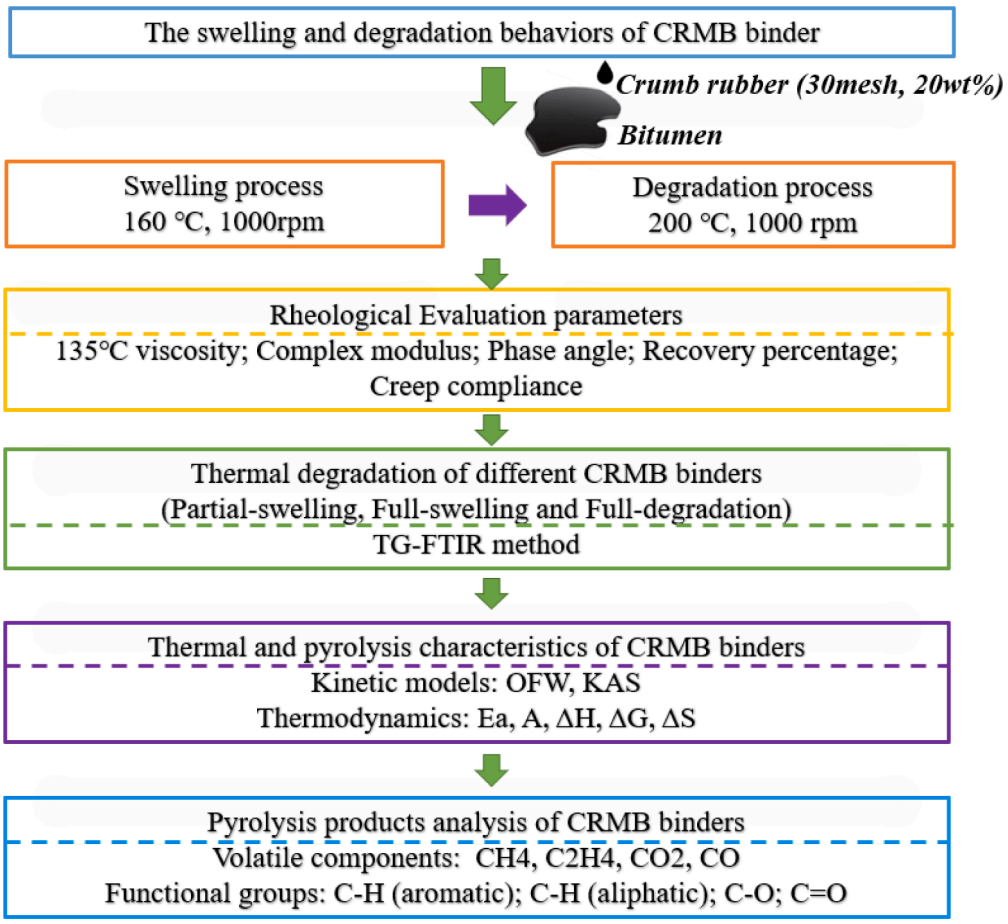

Fig. 1. The research protocol of this study.

Brookfield Engineering Laboratories, Inc., USA) device with a #27 cylindrical rotor was employed to measure the 135 °C viscosity values of CRMB binders during its swelling and degradation processes (AASHTO T316-13) [32]. The sample weight in the aluminum tube and the spinning rate was 10.5 g and 20 rpm, respectively.

The rheological parameters of CRMB binders were characterized through a DSR (TA-HR1, TA Instruments Company, USA) with a parallel diameter of 25 mm and gap width of 1 mm (AASHTO M320) [33]. The frequency sweep tests (0.01–100 rad/s, 60 °C) were conducted to estimate the complex modulus (G*) and phase angle (δ) of various CRMB binders. Moreover, the 60 °C multiple stress creep and recovery (MSCR) tests with the stress levels of 0.1 and 3.2 kPa were carried out to determine the recovery percentage (R%) and non-recoverable creep compliance (J_{nr}) of CRMB binders (AASHTO TP70) [34].

2.3.2. TG-FTIR test

In this study, the pyrolysis behaviors and volatile components of the CRMB binders with various swelling-degradation degrees were detected using the thermogravimetric analyzer (STA 449F3-TGA, manufactured from NETZSCH Company, Germany) connected with Fourier Transform Infrared spectrometer (TENSOR II-FTIR, produced by the Bruker Optics, Germany). Non-isothermal TGA could be utilized to achieve the solid waste pyrolysis procedure, and the system temperature increased from 25 to 900 °C with a constant rate of 100 °C /min. The inert atmosphere was the ultrahigh purity nitrogen (99.999 %, N_2) with the flow rate of 100 ml/min (the ratio of purge gas and protective gas is 80/20). About 10 mg sample was placed in an alumina crucible and thermal analytical balance was conducted before analysis.

In addition, the pyrolysis gas products during the TGA process were transferred to the FTIR device to probe the chemical components through a polytetrafluoroethylene transfer line, which was heated at 200 °C to prevent the condensation of volatiles. The FTIR spectrum of the gas product was collected in a special range of 4000–400 cm^{-1} with a resolution of 4 cm^{-1} and scan times of 12. To ensure accuracy, all characterization tests for each sample were implemented at least two times.

3. Pyrolysis kinetic models

Generally, during the pyrolysis process, the mass percentage of the CRMB sample decreases gradually as the system temperature rises at a constant rate. The thermal conversion rate of the CRMB specimen is calculated as follows:

$$\alpha = \frac{m_0 - m_t}{m_0 - m_f} \tag{1}$$

where α refers to the reaction conversion; m_0, m_t and m_f is the sample mass at the initial, time t, and final point, respectively.

In the isothermal duration, the basic equation can be utilized to express the correlation between the reaction conversion α and pyrolysis time t:

$$\frac{d\alpha}{dt} = kf(\alpha) \tag{2}$$

where the parameter k represents the rate of mass loss, and it is temperature dependence; $f(\alpha)$ represents a mathematical function of the reaction mechanism. Moreover, the Arrhenius equation is adopted to describe the correlation between the parameter k and temperature T:

Table 3
Common solid-state thermal reaction models (Xu et al., 2018).

Reaction mechanism	Code	*f*(a)	*g*(a)
First order	F1	$1-\alpha$	$-\ln(1-\alpha)$
Second order	F2	$(1-\alpha)^2$	$(1-\alpha)^{-1}-1$
Third order	F3	$(1-\alpha)^3$	$[(1-\alpha)^{-1}-1]/2$
One-dimension diffusion	D1	$1/2\alpha^{-1}$	α^2
Two-dimension diffusion	D2	$[-\ln(1-\alpha)]^{-1}$	$(1-\alpha)\ln(1-\alpha)+\alpha$
Three-dimension diffusion	D3	$\frac{3}{2(1-\alpha)}\frac{2}{3}(1-(1-\alpha)^{1/3})^{-1}$	$[1-(1-\alpha)^{1/3}]^2$
Three-dimension diffusion	D4	$3/2[(1-\alpha)^{-1/3}-1]$	$1-\frac{2}{3\alpha}-(1-\alpha)^{2/3}$
Two-dimension nucleation	A2	$2(1-\alpha)[-\ln(1-\alpha)]^{1/2}$	$[-\ln(1-\alpha)]^{1/2}$
Three-dimension nucleation	A3	$3(1-\alpha)[-\ln(1-\alpha)]^{2/3}$	$[-\ln(1-\alpha)]^{1/3}$
One-dimension phase boundary	R1	1	α
Contracting sphere	R2	$2(1-\alpha)^{1/2}$	$1-(1-\alpha)^{1/2}$
Contracting cylinder	R3	$3(1-\alpha)^{2/3}$	$1-(1-\alpha)^{1/3}$

$$k = A\exp\left(-\frac{E_a}{RT}\right) \tag{3}$$

where A represents the pre-exponential factor; E_a is the activation energy and R refers to the gas constant, 8.314 $J\cdot mol^{-1}\cdot K^{-1}$.

By combining the Eqs. (2) and (3), the reaction rate $\frac{d\alpha}{dt}$ can be expressed in the following equation:

$$\frac{d\alpha}{dt} = A\exp\left(-\frac{E_a}{RT}\right)f(\alpha) \tag{4}$$

We assume that the parameter β represents the heating rate of TGA pyrolysis:

$$\beta = \frac{dT}{dt} \tag{5}$$

Hence, Eq. (4) can be rewritten as follows:

$$\beta\frac{d\alpha}{dT} = A\exp\left(-\frac{E_a}{RT}\right)f(\alpha) \tag{6}$$

By further simultaneous integration of both sides, Eq. (6) is expressed as shown:

$$g(\alpha) = \int_0^{\alpha}\frac{d\alpha}{df(\alpha)} = \left(\frac{A}{\beta}\right)\int_{T_0}^{T}\exp\left(-\frac{E_a}{RT}\right)dT \tag{7}$$

To describe the thermal pyrolysis kinetic of CRMB binder, two common kinetic models are employed, including the Ozawa-Flynn-Wall (OFW) method and Kissinger-Akahira-Sunose (KAS) method. And the information of the two mathematic models is introduced herein.

The OFW model comes from the integral method with a Doyle's approximation, and the detailed equation is described below:

$$\ln\beta = \ln\left[\frac{AE_a}{Rg(\alpha)}\right] - 5.331 - \frac{1.052E_a}{RT} \tag{8}$$

By formula processing, Eq. (9) is obtained:

$$\ln g(\alpha) = \ln\left[\frac{AE_a}{\beta R}\right] - 5.331 - \frac{1.052E_a}{RT} \tag{9}$$

Therefore, the activation energy E_a and pre-exponential factor A for the CRMB binder pyrolysis can be determined by plotting $\ln g(\alpha)$ vs 1/T with the temperature increasing rate of 100 °C /min. The related slope and intercept values are $(-\frac{1.052E_a}{R})$ and $\ln\left[\frac{AE_a}{\beta R}\right] - 5.331$, respectively.

Regarding the KAS method, another Coats-Redfern approximation is applied and the relationship between g(α) and temperature T is as follows:

$$\ln\frac{\beta}{T^2} = \ln\left[\frac{AR}{E_a g(\alpha)}\right] - \frac{E_a}{RT} \tag{10}$$

Similarly, the simplified KAS model is shown as the following formula:

$$\ln g(\alpha) = \ln\left[\frac{AR}{E_a}\right] - \ln\left[\frac{\beta}{T^2}\right] - \frac{E_a}{RT} \tag{11}$$

Lastly, the parameters of activation energy E_a and pre-exponential factor A can be determined by fitting the correlation curve of g(α) and temperature T.

To this end, it is important to understand the pyrolysis reaction model f(α) and its integral form g(α), shown in Eq. (7). The pyrolysis reaction of the CRMB binder is complex, and some common solid-state thermal reaction models are adopted and displayed in Table 3. In this study, the mass variety of CRMB detected during the pyrolysis procedure is utilized to calculate the conversion parameter α. And then the correlation curve between g(α) and temperature can be drawn using different thermal reaction models. Through fitting these curves with the OFW and

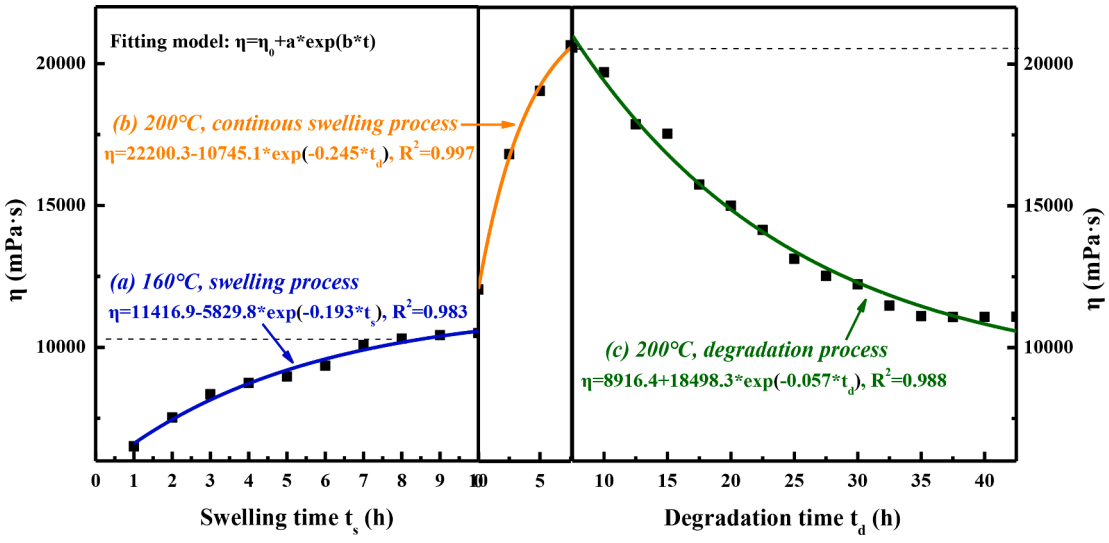

Fig. 2. The viscosity value of 30mesh CRMB during swelling(a) and degradation(b) processes.

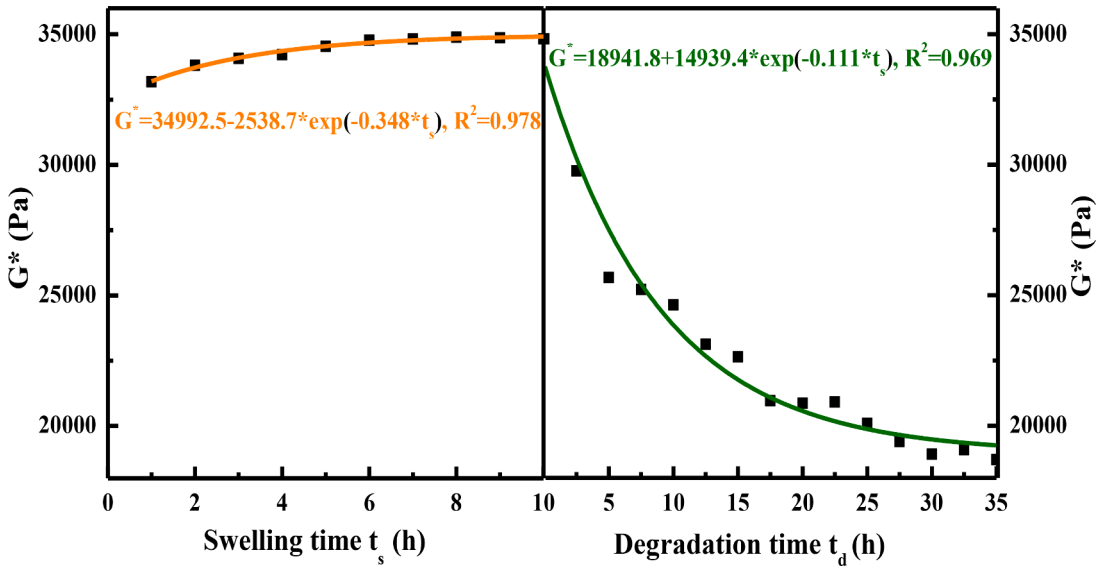

Fig. 3. The relationships between G* value of CRMB with swelling and degradation time.

KAS methods, the activation energy E_a and pre-exponential factor A can be determined.

Further, the thermodynamic parameters of CRMB binder during its pyrolysis process are calculated as shown in Eqs. (12)-(14), which includes the enthalpy (ΔH), Gibbs free energy (ΔG), and entropy (ΔS).

$$\Delta H = E_a - RT \tag{12}$$

$$\Delta G = E_a + RT_{max}\ln\left(\frac{K_B T_{max}}{hA}\right) \tag{13}$$

$$\Delta S = (\Delta H - \Delta G)/T_{max} \tag{14}$$

where the E_a and A are both obtained from kinetic models, K_B is the Boltzmann constant ($1.381*10^{-23}$ $J{\cdot}K^{-1}$), and h refers to the Planck's constant, $6.626*10^{-34}$ $J{\cdot}s^{-1}$.

4. Results and discussion

4.1. The viscosity variation of CRMB binder during swelling-degradation stages

The rotational viscosity η at 135 °C of the CRMB binder was tested during its continuous swelling and degradation processes. Fig. 2(a) and (b) illustrate the viscosity variation as a function of swelling time t_s and degradation time t_d, respectively. It shows that the viscosity value of CRMB increases gradually with the increase of swelling time, which is attributed to the volume extension of CR particles due to light oil absorption. The molecules of bitumen components with light-weight continuously diffuse into rubber particles with the driving force of concentration gradient until reaching the equilibrium state at 160 °C. Interestingly, the viscosity value of the CRMB binder tends to be stable when the swelling time exceeds 8 h. It means that the swelling equilibrium state of CRMB is obtained when the swelling time is 8 h, and the equilibrium-swelling viscosity is 10.5 Pa·s. From the perspective of microscopic, the low-weight oily fractions' concentration in rubber particles is the same as that in bitumen matrix, and the dynamic equilibrium reaction is obtained.

Once the swelling and degradation temperature rises from 160 to 200 °C, the viscosity of the CRMB binder at 135 °C enlarges significantly. High temperature accelerates the diffusion capacity improvement of bitumen components and increases the swelling degree of crumb rubber in bitumen. In detail, the viscosity of the CRMB binder reaches the maximum value of 20.58 Pa·s when the degradation time is 7.5 h, which is approximately two times larger than that of the full-swelling one. At this point, the swelling degree of the CRMB binder is considered to be the highest, which is then subjected to the degradation procedure. When the degradation time exceeds 7.5 h, the viscosity value of the CRMB binder expectedly reduces gradually, which proves the degradation occurrence of CRMB at 200 °C. At this stage, the polymer network of crumb rubber is destroyed and dissolved in the bitumen matrix.

When the degradation duration is about 35 h, the 135 °C rotational viscosity keeps stable at 11.09 Pa·s. As expected, the full-degradation CRMB is more homogenous and exhibits better workability. It can be found that the degradation time at 200 °C is much longer than the swelling time, which could be accelerated by increasing the degradation temperature. For instance, the preparation temperature of terminal blend rubber bitumen was higher than 200 °C to shorten the degradation time. Interestingly, the viscosity values of full-degradation and full-swelling CRMB binders at 160 °C are close. It implies that the full-swelling effect at 160 °C on viscosity is similar to the full-degradation influence at 200 °C. However, the interaction mechanism is totally different. The former is due to the adsorption of light oily fractions and the volume expansion of CR particles, but the latter is associated with the release of CR components into the bitumen matrix.

The exponential equation, shown in Eq. (15), is adopted to quantitively probe the rheological indices variety as a function of the swelling/degradation time. The whole swelling and degradation process of the CRMB binder is divided into three stages, including the stable swelling, continuous swelling, and stable degradation steps.

$$Y = a + b*\exp(c*t) \tag{15}$$

where Y refers to the rheological indicators (η, G*, δ, R% or J_{nr}), t represents the swelling or degradation time, and a, b, c are constants.

The exponential formulas are presented in Fig. 2. The absolute "b" value of 0.193 in the 160 °C swelling curves is lower than that in 200 °C, because the high temperature would promote the swelling rate and shorten the equilibrium swelling time of the CRMB binder. Besides, the swelling time decreases with the temperature increases, and the swelling process of CR particles in bitumen is difficult to observe when the temperature is extremely high. The absolute "b" value during the degradation process is the lowest, indicating the degradation rate is much lower than the swelling rate.

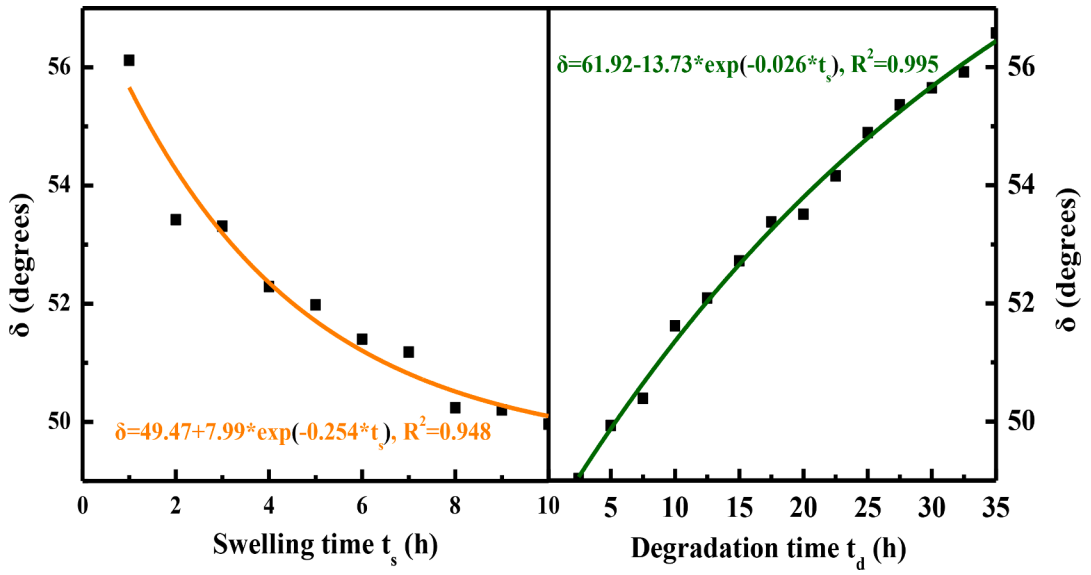

Fig. 4. The relationships between phase angle of CRMB binder with swelling time and degradation time.

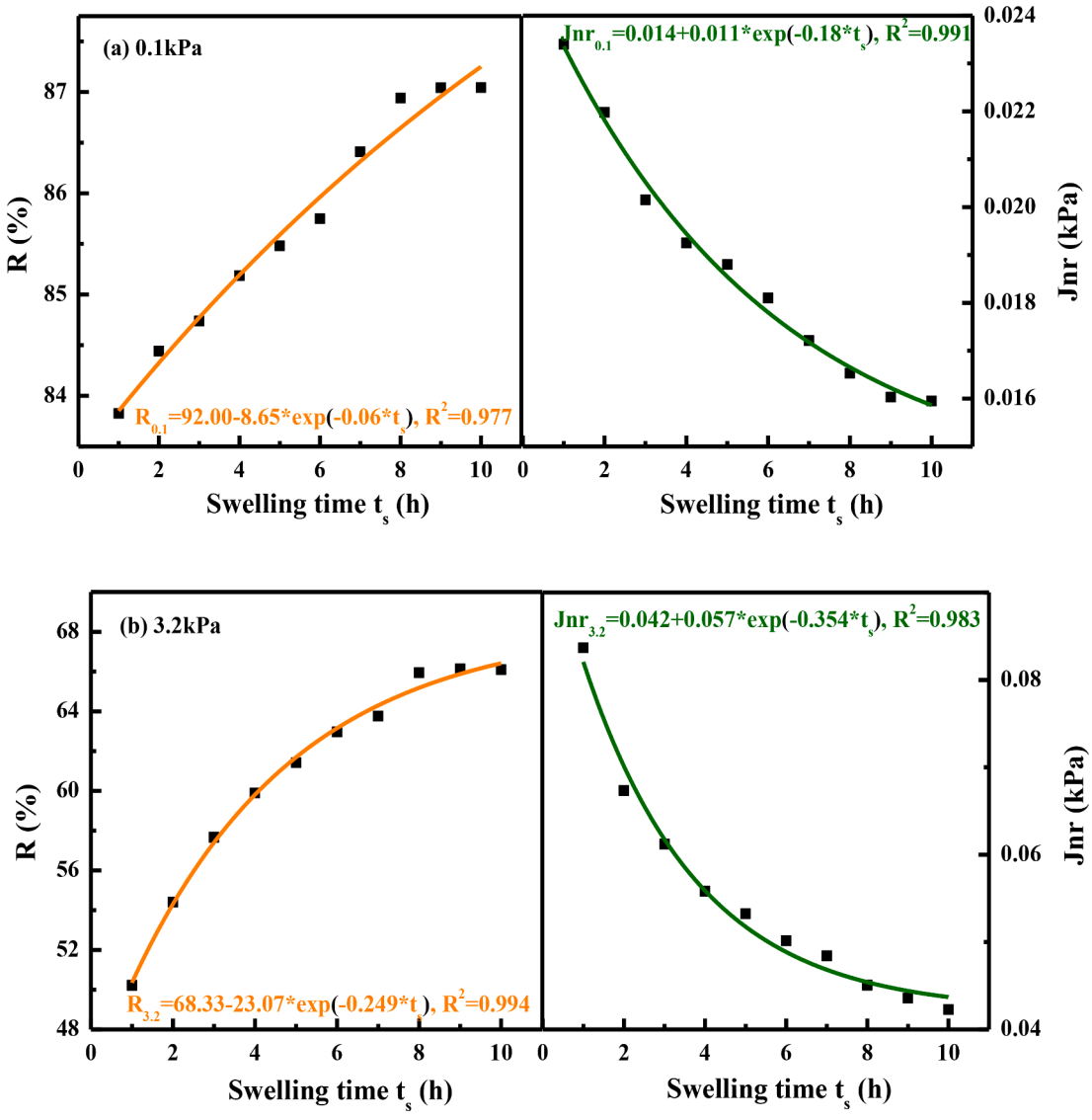

Fig. 5. The relationships between R% and Jnr of CRMB binder with swelling time at (a) 0.1 and (b) 3.2 kPa.

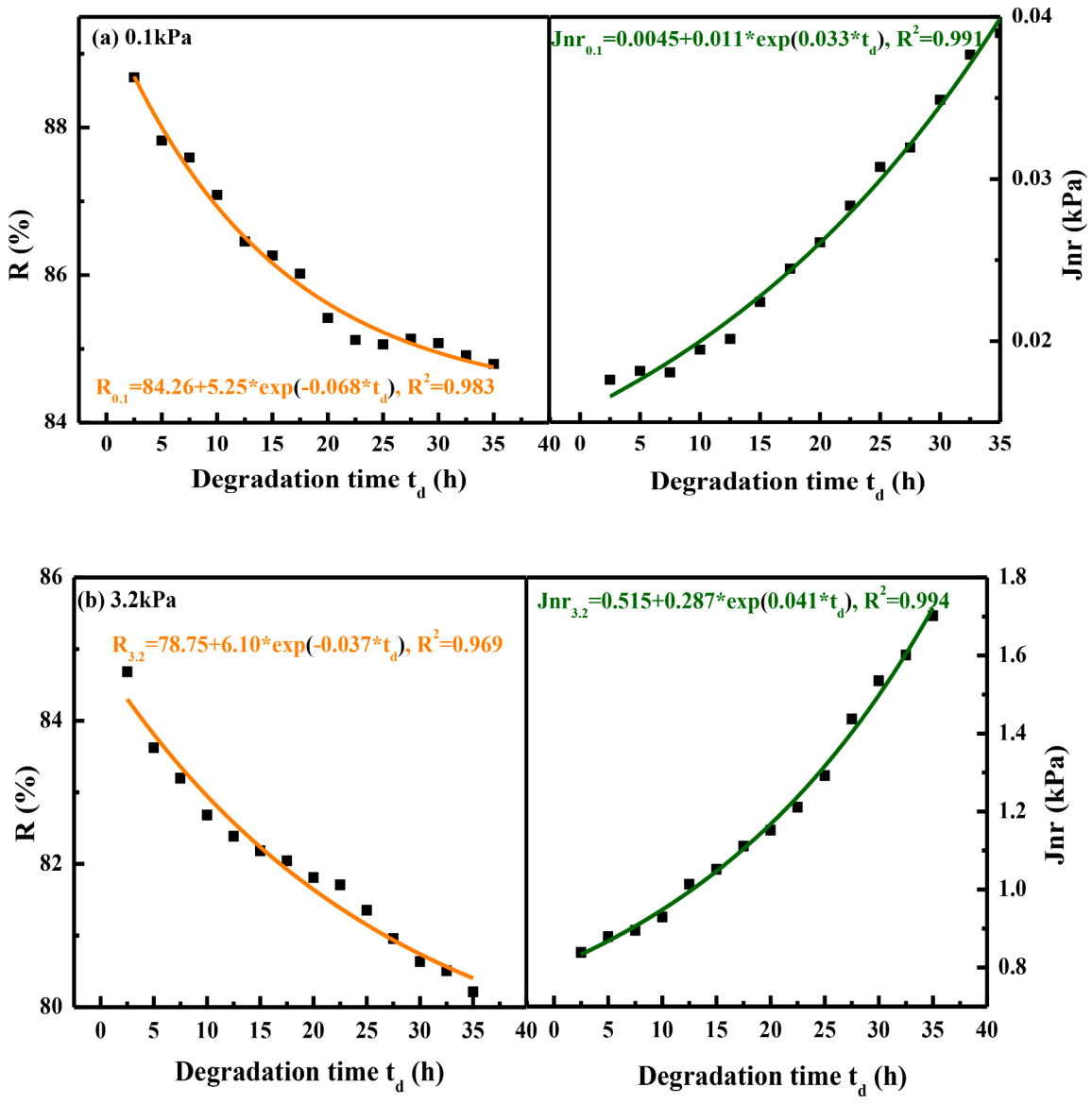

Fig. 6. The relationships between R% and Jnr of CRMB binder with degradation time at (a) 0.1 and (b) 3.2 kPa.

4.2. Influence of swelling and degradation on rheological properties of CRMB binder

*4.2.1. Complex modulus G**

To present the G* value variety of CRMB binder during the swelling and degradation processes, Fig. 3 illustrates the G* of CRMB binders at 10 rad/s and 60 °C. The exponential function can fit the correlation curve between the G* value and swelling time t_s or degradation time t_d well, simultaneously. The G* of the CRMB binder increases slightly during the swelling process, while it declines as the increase of degradation duration dramatically.

It is interesting to note that the variation rate of G* to the swelling/degradation time significantly differs from the aforementioned viscosity results. The rotational viscosity of the CRMB binder increases gradually till reaching an equilibrium state at 160 °C, which continues to enlarge to the maximum value within the first 7.5 h when the system temperature rises to 200 °C instantly. From Fig. 3, although the overall change trend of G* is similar to η, the intermediate stage could not be observed. When the temperature rises to 200 °C, the G* of the CRMB binder immediately decreases.

Additionally, the G* of full-degradation CRMB is far lower than the full-swelling and initial CRMB specimens. It implies that the complex modulus would remarkably deteriorate during the degradation process. The CRMB binder exhibits the high-viscosity characteristic although it reaches the equilibrate degradation status, which results in a high temperature required for the preparation, mixing, and compaction of rubber bitumen and asphalt. The high degradation depth would seriously decrease the complex modulus and stiffness of the CRMB binder.

4.2.2. Phase angle δ

The phase angle δ is an important indication to estimate the viscoelastic response of bitumen, and the high δ value reflects that the bitumen exhibits mainly viscous characteristic. The correlation curves of δ-t_s and δ-t_d at 10 rad/s and 60 °C are illustrated in Fig. 4. The phase angle declines as the swelling time increases, while it increases gradually during the degradation process. It indicates that the swelling procedure enhances the elastic performance, and the degradation process increases the viscous friction of the CRMB binder. During the swelling process, the rubber particles absorb the oily constitutes and its volume continues to increase. The rubber network is inflated like a balloon and its self-elasticity is enhanced. At the same time, the relative distance and interaction between rubber particles are reduced and improved. That's

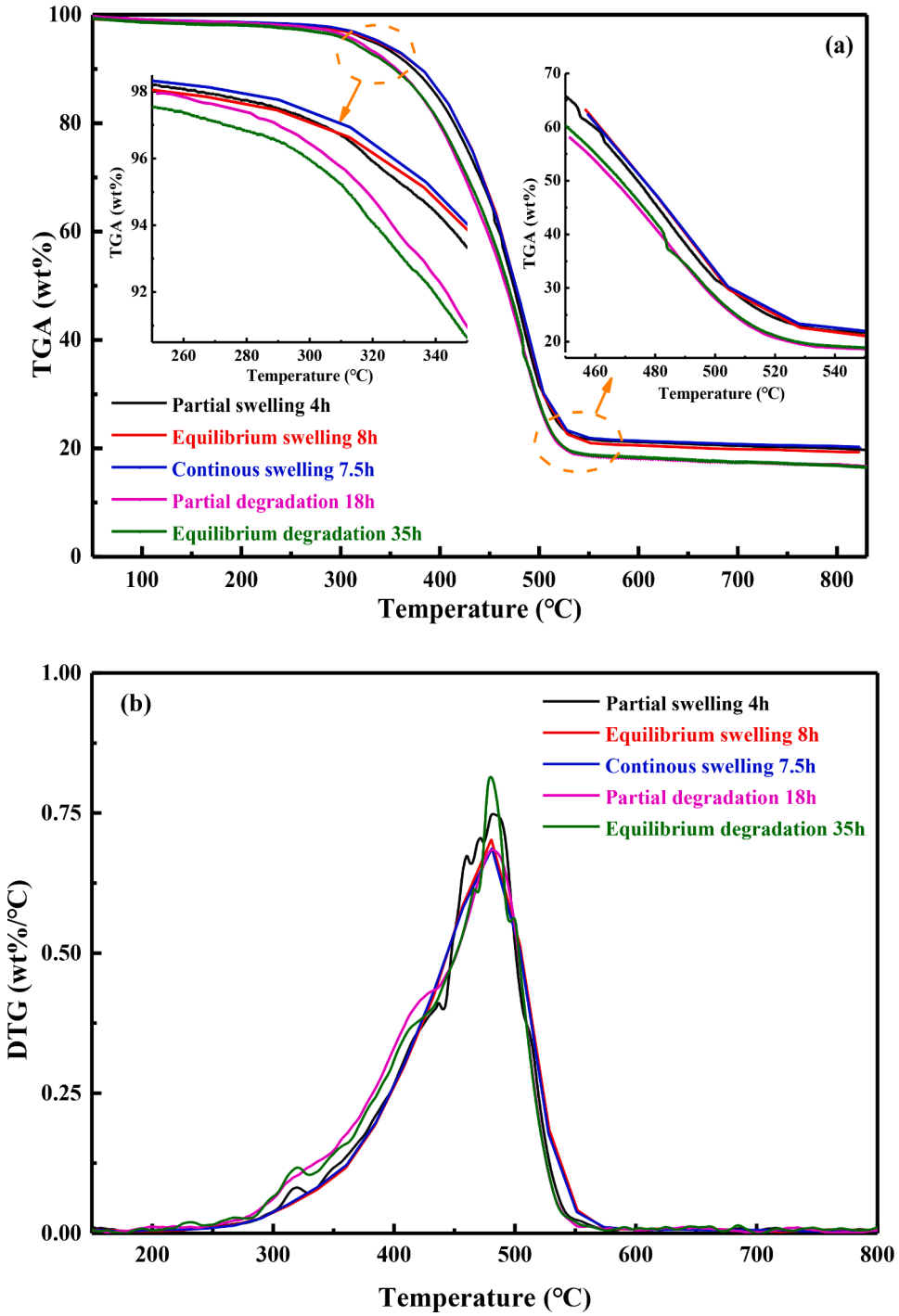

Fig. 7. TG (a) and DTG (b) curves of CRMB binders with different swelling and degradation degrees.

why the elastic characteristic of the CRMB binder is strengthened during the swelling process. On the other hand, when the CRMB binder is subjected to degradation duration, the polymer network structure is damaged, and the inner components are dissolved into the bitumen matrix. The elasticity provided by solid rubber particles and stiff bitumen matrix is weakened, while the increased sticky substance in the bitumen matrix enlarges the viscous friction of the CRMB binder. Based on the δ values higher than 50°, the CRMB binder is dominated by the viscous characteristic regardless of the swelling and degradation degree.

The phase angle curves are fitted by the exponential functions with R^2 values higher than 0.94. The absolute "b" value in the swelling curve is much higher than the degradation curve, indicating the variation rate of phase angle in the swelling process is faster. Compared with the viscosity and complex modulus, the phase angle variety of CRMB binder is slower, because the solid matter from crumb rubber, such as carbon black, cannot be dissolved in the bitumen matrix. Besides, the continuous descending point at 2.5 h in the degradation curve could be observed, which is due to the continuous swelling of rubber particles when the reaction temperature rises from 160℃ to 200 °C. Afterward, the δ value starts to rise due to the increment of viscous fractions.

When the degradation time is 35 h, the phase angle of the CRMB binder has a continuing upward trend. Although the viscosity and complex modulus both reach the equilibrium state, the phase angle has no clear equilibrium point. The viscous components and the ratio of loss

and elastic modulus in the CRMB binder would continue to increase after the full-degradation time. It is interesting to mention that the δ value of the full-degradation sample is similar to the initial-swelling specimen, which is 56° approximately. However, their swelling-degradation degrees of these two CRMB samples are different even though their viscoelastic ratios are at the same level. In other words, the contributions of crumb rubber and bitumen matrix to the viscoelastic ratio are significantly different.

4.2.3. Recovery percentage R% and creep compliance J_{nr}

Fig. 5 plots the R% and J_{nr} values of CRMB binders as the function of swelling time t_s. The R% parameter decreases and the J_{nr} value increases as the applied stress level increases from 0.1 to 3.2 kPa, and the reason is attributed to the larger deformation level under high loading stress. It is worth noting that the R% value increases during the swelling process, while the corresponding J_{nr} value decreases. The outcome agrees well with the aforementioned phase angle result that the CRMB binder with a higher swelling degree exhibits an improved elastic behavior. The enhanced recovery capacity is related to the volume expansion of rubber particles and the absorption of viscous oily components from the bitumen matrix. The high swelling degree is beneficial to strengthen the elastic recovery and resistance to the permanent deformation of the CRMB binder. In addition, the influence of swelling degree on MSCR parameters of CRMB depends on the applied stress value. At the stress level of 0.1 kPa, the R% value of the full-swelling sample is 3.8 % higher than that of the initial swelling specimen, and the J_{nr} value of the former decreases by approximately 30 % when it reaches the equilibrium swelling state. When the applied stress is 3.2 kPa, the corresponding percentage of R% increment and J_{nr} reduction is 32 % and 49 %, respectively.

The exponential function is adopted to draw the correlation curves of swelling time and MSCR parameters (R% and J_{nr}). The absolute "b" value in the R% curve is lower than that in the J_{nr} curve. Hence, the swelling influence on the J_{nr} value is more significant than R%, regardless of the stress level. From the perspective of the high-temperatures properties of the CRMB binder, the full-swelling sample is recommended. On the other hand, the R% and J_{nr} parameters during the degradation procedure are measured and presented in Fig. 6. The degradation effect is converse to the swelling case. With the degradation time prolonging, the R% and J_{nr} of CRMB binder decreases and increases, respectively. This phenomenon is due to the increase of viscous components in the bitumen matrix released from the rubber phase. Compared with the initial degradation sample (2.5 h), the R% of the full-degradation specimen (35 h) decreases by 4.39 % (at 0.1 kPa) and 5.28 % (at 3.2 kPa), while the J_{nr} value increases by 1.21 and 1.03 times. It is summarized that the degradation operation shows a greater influence on J_{nr} than R% of the CRMB binder.

In addition, the R% values of the initial and full degradation samples at 0.1 kPa are 4.5 % and 5.4 % higher than that at 3.2 kPa. Moreover, the corresponding J_{nr} value increases by 46.6 and 42.7 times, indicating that the stress level displays a greater influence on the J_{nr} than R%. According to the absolute "b" values, the variable rate of R% to the degradation time is faster than J_{nr} at 0.1 kPa, but the former is lower than the latter at 3.2 kPa. When the stress increases, the variable rate of R% and J_{nr} decreases and increases, respectively.

As the degradation duration prolongs, the J_{nr} value of the CRMB binder increases significantly. There is no equilibrium J_{nr} value observed, and the J_{nr} continues to increase when the degradation time reaches 35 h. It means that the non-recoverable viscous part still increases when the shear viscosity and complex modulus reach the equilibrium state. This finding agrees with the aforementioned phase angle result. Therefore, when the degradation time exceeds the full-degradation point (35 h), the rheological parameters of viscosity, complex modulus, and rutting parameter keep constant, but the viscous components continue to increase.

Table 4
Pyrolysis characteristics of CRMB binders during swelling and degradation degrees.

CRMB samples	PS 4 h	ES 8 h	CS 7.5 h	PD 18 h	ED 35 h
T_s (℃)	40.3	42.7	43.9	31.3	28.8
Residue Re (wt%)	19.37	19.98	20.38	17.05	16.93
T_{DTGmax} (℃)	485.2	480.5	481.0	481.3	479.8
DTG_{max} (wt%/℃)	0.746	0.703	0.685	0.687	0.815

Note: PS—partial swelling; ES—equilibrium swelling; CS—continuous swelling; PD—partial degradation; and ED—equilibrium degradation.

4.3. TG/DTG analysis

The Thermogravimetry (TGA) and corresponding differential of thermogravimetry (DTG) curves of CRMB binders are displayed in Fig. 7a and b. From Fig. 2, the swelling-degradation duration of CRMB with various swelling-degradation degrees can be determined. To investigate the influence of swelling-degradation degree on the thermal pyrolysis behaviors of CRMB binder, some representative samples with different swelling-degradation levels are selected. The equilibrium-swelling, continuous-swelling, equilibrium-degradation points of CRMB binders can easily be found in Fig. 2, and their preparation time is 8 h, 7.5 h, and 35 h, respectively. It should be mentioned that the equilibrium-swelling and equilibrium-degradation CRMB binders are also called full-swelling and full-degradation samples. Meanwhile, the partial-swelling and partial-degradation CRMB binders are chosen and prepared with the swelling time of 4 h and degradation time of 18 h, which are half-values of preparation time of full-swelling and full-degradation samples.

For all CRMB samples, only one pyrolysis stage in the TGA curve and one peak in the DTG curve are observed. From the TGA curve, the mass weight of the CRMB binder shows no obvious change when the temperature is lower than 300 °C. Afterward, the TGA curve drops down with the increase of temperature dramatically, which refers to the thermal degradation of the CRMB sample. When the temperature exceeds 520 °C, the mass weight keeps constant and the residue percentage is measured. The CRMB binders during the swelling and degradation processes display different start-point, pyrolysis rate, and end-point in TGA curves. To further analyze the difference, the fractional TGA curves around the pyrolysis start and end-points are enlarged. When the pyrolysis is the same, the mass weight of the CRMB binder increases and decreases as the swelling and degradation degrees deepens. Moreover, the order regarding the rate of mass change for CRMB binders is full-degradation > partial degradation > partial swelling > full swelling > maximum swelling. The thermal degradation temperature region and the temperature with the maximum pyrolysis rate of the CRMB binders are obtained in the DTG curves. The pyrolysis rate of the CRMB binder increases first and then decreases, whilst the temperature regions of increasing and decreasing DTG are about 250–480 °C and 480–550 °C, respectively.

Table 4 lists the pyrolysis parameters of CRMB binders with various swelling and degradation levels, including the pyrolysis start temperature T_s, maximum DTG value DTG_{max}, corresponding temperature T_{DTGmax}, and residue percentage Re. As the swelling degree enlarges, the T_s value increases from 40.3 to 43.9 °C, which distinctly decreases as the degradation degree deepens. The CRMB binder at the equilibrium degradation of 35 h exhibits the lowest pyrolysis-start temperature of 28.8 °C, while the continuous swelling 7.5 h sample has the highest T_s value. It demonstrates that the swelling process hinders the thermal degradation, while the degradation duration promotes the pyrolysis degree of the CRMB binder. Meanwhile, the residue percentage of swelled CRMB binders is all larger than that of degraded samples. It can be concluded that the swelling procedure would be beneficial to improve the thermal stability of the CRMB binder, which deteriorates gradually during the degradation process.

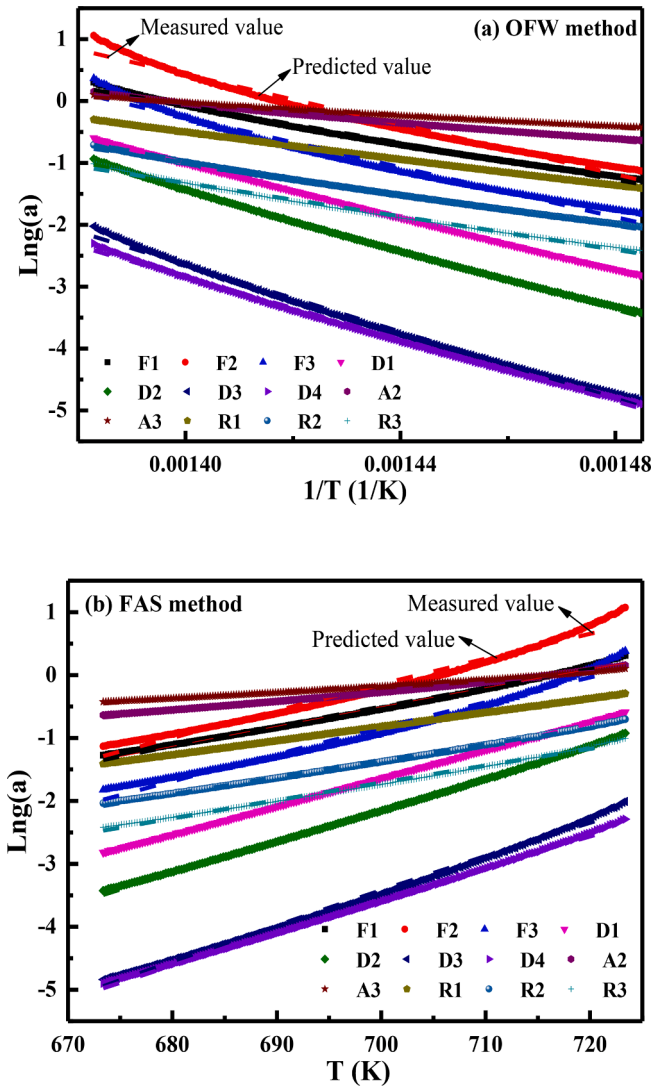

Fig. 8. The kinetic analysis of partial-swelling CRMB binder using OFW (a) and FAS (b) methods.

Additionally, all samples show similar T_{DTGmax} values around the region of 479–485 °C when the pyrolysis rate reaches the maximum point, while the swelling and degradation degree has no significant influence on the T_{DTGmax} value of the CRMB binder. However, the DTG_{max} parameter of CRMB binders with various swelling and degradation degrees differ dramatically. With the increase of swelling degree, the DTG_{max} value distinctly decreases, while it increases during the degradation process. The reason is that the light-weight oily fractions in bitumen are absorbed in the rubber phase, and the rubber network provides a protective barrier to hinder the thermal degradation of small molecules. Meanwhile, the absorbed components promote the volume expansion and elasticity improvement of crumb rubber. On the contrary, the rubber network in degradation CRMB binder is damaged and oily fractions are released into the bitumen matrix.

The OFW and KAS methods are adopted to fit the correlation curves between the conversion rate α and pyrolysis temperature T using twelve thermal reaction models, listed in Table 3. Fig. 8 illustrates the experimental and fitting curves of the partial-swelling CRMB binder, which demonstrates that the OFW and KAS methods together with the thermal reaction models both fit the kinetic curves well. The activation energy Ea, pre-exponential factor A and correlation coefficient R^2 of the partial-swelling, full-swelling, and full-degradation CRMB binders are calculated and displayed in Tables 5-7. The R^2 values higher than 0.94

Table 5
The kinetic parameters of partial-swelling CRMB binder by OFW and KAS methods.

Model	OFW method			KAS method		
	Ea/ kJ·mol^{-1}	A/min^{-1}	R^2	Ea/ kJ·mol^{-1}	A/min^{-1}	R^2
F1	118.27	8.19E + 06	0.9921	113.11	4.63E + 08	0.9920
F2	159.05	1.38E + 10	0.9784	156.40	1.55E + 12	0.9779
F3	159.05	6.91E + 09	0.9784	156.40	7.78E + 11	0.9779
D1	171.19	2.91E + 10	0.9996	169.20	3.45E + 12	0.9996
D2	190.73	4.89E + 11	0.9982	189.26	7.35E + 13	0.9982
D3	213.10	6.84E + 12	0.9955	212.96	1.33E + 15	0.9955
D4	198.15	4.28E + 11	0.9974	197.11	7.04E + 13	0.9974
A2	59.13	4.80E + 02	0.9921	50.75	5.94E + 03	0.9922
A3	39.42	2.22E + 01	0.9921	29.97	1.07E + 02	0.9923
R1	85.90	2.37E + 04	0.9996	78.80	6.50E + 05	0.9996
R2	101.04	1.81E + 05	0.9969	94.84	7.16E + 06	0.9969
R3	106.55	3.27E + 05	0.9955	100.68	1.46E + 07	0.9955

Table 6
The kinetic parameters of full-swelling CRMB binder by OFW and KAS methods.

Model	OFW method			KAS method		
	Ea/ kJ·mol^{-1}	A/min^{-1}	R^2	Ea/ kJ·mol^{-1}	A/min^{-1}	R^2
F1	95.28	8.90E + 04	0.9873	88.14	2.76E + 06	0.9878
F2	140.03	2.35E + 08	0.9416	135.21	1.64E + 10	0.9425
F3	140.03	1.17E + 08	0.9416	135.21	8.20E + 09	0.9425
D1	127.59	5.50E + 06	0.9982	122.31	3.16E + 08	0.9980
D2	144.63	5.91E + 07	0.9999	140.06	4.42E + 09	0.9999
D3	166.67	6.84E + 08	0.9961	163.24	6.87E + 10	0.9963
D4	151.88	4.80E + 07	0.9993	147.68	3.97E + 09	0.9994
A2	47.64	5.57E + 01	0.9873	38.02	3.73E + 02	0.9884
A3	31.76	5.68E + 00	0.9873	21.31	1.42E + 01	0.9890
R1	63.80	3.79E + 02	0.9982	55.02	4.91E + 03	0.9978
R2	77.92	2.17E + 03	0.9987	69.88	4.35E + 04	0.9989
R3	83.33	3.69E + 03	0.9961	75.57	8.59E + 04	0.9965

validates the reliability of calculated kinetic parameters. Interestingly, the R^2 values of full-degradation CRMB binders are all higher than 0.999, indicating that the kinetic models are more applicable to the CRMB sample as the degradation degree deepens. Besides, the calculated Ea and A parameters of the CRMB binder remarkably depend on the type of thermal kinetic and reaction models, especially for the pre-exponential factor. Compared to the OFW method, the Ea value from the KAS method is lower, but the A parameter is significantly higher regardless of the reaction model type and swelling-degradation degree of CRMB. The thermal reaction model affects the kinetic parameters of CRMB, and both Ea and A present the same law of change as the reaction

Table 7
The kinetic parameters of full-degradation CRMB binder by OFW and KAS methods.

Model	OFW method			KAS method		
	Ea/ kJ·mol^{-1}	A/min^{-1}	R^2	Ea/ kJ·mol^{-1}	A/min^{-1}	R^2
F1	64.45	7.66E + 02	0.9999	57.25	1.15E + 04	0.9999
F2	80.51	1.20E + 04	0.9993	73.09	2.83E + 05	0.9994
F3	80.51	5.99E + 03	0.9993	73.09	1.42E + 05	0.9993
D1	104.92	1.70E + 05	0.9993	98.77	7.09E + 06	0.9993
D2	112.91	3.85E + 05	0.9997	107.18	1.88E + 07	0.9996
D3	121.78	4.57E + 05	0.9999	116.51	2.61E + 07	0.9999
D4	115.86	1.49E + 05	0.9998	110.28	7.67E + 06	0.9997
A2	32.72	6.24E + 00	0.9999	22.82	1.87E + 01	0.9999
A3	21.82	1.49E + 00	0.9999	11.35	1.49E + 00	0.9999
R1	52.46	7.35E + 01	0.9993	43.58	6.75E + 02	0.9992
R2	58.70	1.13E + 02	0.9998	50.15	1.33E + 03	0.9998
R3	60.89	1.12E + 02	0.9999	52.45	1.43E + 03	0.9998

model. Based on the correlation coefficient R^2 values, the reaction models of D1, R1, and D2 are more suitable for swelling CRMB binder, while the fitting curves of degradation CRMB with the F1, D3, A2, and A3 reaction models are more accurate.

It can be found that the Ea and A parameters of all CRMB binders reach the maximum values in the D3 model while showing the minimum points in the A3 model. In detail, the activation energy Ea values of the partial-swelling, full-swelling, and full-degradation CRMB binders in the OFW method are located in 39.42–213.10, 31.76–166.67, and 21.82–121.78 kJ·mol^{-1}, which are in 29.97–212.96, 21.31–163.24, and 11.35–116.51 kJ·mol^{-1} in KAS model. Meanwhile, the corresponding pre-exponential factor A values cover 22.2 to $6.84*10^{12}$, 5.68 to $6.84*10^{8}$, and 1.49 to $4.57*10^{5}$ min^{-1} in the OFW method, which is from $1.07*10^{2}$ to $1.33*10^{15}$, 14.2 to $6.87*10^{10}$, and 1.49 to $2.61*10^{7}$ min^{-1} in the KAS method. These fluctuations reveal that the pyrolysis kinetic and thermal reaction models should be optimized and validated. Additionally, the Ea and A values of degradation CRMB binder are both lower than that of the swelling sample. It means that lower energy is needed for the degradation CRMB binder to perform the thermal pyrolysis.

Furthermore, three thermodynamic parameters of enthalpy (ΔH), Gibbs free energy (ΔG), and entropy (ΔS) during the thermal pyrolysis of CRMB binders are displayed in Tables 8 and 9. The ΔH parameter reflects the energy difference between the pyrolysis products and reactants, and the ΔG factor is the total internal energy of the reaction system. Moreover, the ΔS refers to the difference in the level of confusion between the reactants and products. The ΔH and ΔG values of all CRMB binders from the OFW method are higher than that from the KAS method, while the ΔS value is lower. On the other hand, the difference between ΔH and Ea of CRMB binders is very small, showing that the thermal reaction is feasible to occur and the external energy mainly contributes to the thermal reaction. In addition, the ΔH values of all CRMB samples are positive, which implies that the pyrolysis process belongs to the endothermic reaction. Moreover, the swelling and degradation degree exhibits a significant influence on the thermodynamic parameters. The ΔH value of degradation CRMB binder is much lower than that of swelling one. This verifies that the energy difference

Table 8
The thermodynamic parameters of different CRMB binders calculated by OFW method.

Model	Partial-swelling CRMB			Full-swelling CRMB			Full-degradation CRMB		
	ΔH (kJ/mol)	ΔG (kJ/mol)	ΔS J/(mol·K)	ΔH (kJ/mol)	ΔG (kJ/mol)	ΔS J/(mol·K)	ΔH (kJ/mol)	ΔG (kJ/mol)	ΔS J/(mol·K)
F1	112.01	212.20	−90.83	89.02	230.68	−128.43	59.19	244.46	−167.97
F2	152.79	184.84	−29.05	133.77	203.19	−62.94	74.25	234.30	−145.11
F3	152.79	191.19	−34.81	133.77	209.54	−68.70	74.25	240.66	−150.87
D1	165.53	190.75	−22.86	121.33	225.17	−94.15	98.66	234.37	−123.04
D2	184.47	183.83	0.59	138.37	220.45	−74.41	106.65	234.87	−116.25
D3	206.84	181.99	22.53	160.41	220.02	−54.04	115.52	242.81	−114.83
D4	191.89	192.45	−0.51	145.62	229.59	−76.13	109.60	246.51	−124.13
A2	52.87	242.43	−171.85	41.38	250.68	−189.76	26.46	255.85	−207.96
A3	33.16	250.91	−197.41	25.50	255.75	−208.75	15.56	258.04	−219.84
R1	79.63	233.41	−139.42	57.74	249.26	−173.82	46.20	252.96	−187.46
R2	94.78	229.92	−122.52	71.66	247.40	−159.33	52.43	255.27	−183.90
R3	100.29	230.02	−117.62	77.07	247.91	−154.88	54.63	257.55	−183.98

Table 9
The thermodynamic parameters of different CRMB binders calculated by KAS method.

Model	Partial-swelling CRMB			Full-swelling CRMB			Full-degradation CRMB		
	ΔH (kJ/mol)	ΔG (kJ/mol)	ΔS J/(mol·K)	ΔH (kJ/mol)	ΔG (kJ/mol)	ΔS J/(mol·K)	ΔH (kJ/mol)	ΔG (kJ/mol)	ΔS J/(mol·K)
F1	106.85	170.03	−57.28	81.88	192.05	−99.88	50.99	211.39	−145.42
F2	150.14	138.88	10.21	128.95	159.43	−27.63	66.83	197.88	−118.81
F3	150.14	145.23	4.46	128.95	165.78	−33.39	66.83	204.23	−124.57
D1	162.94	144.37	16.84	115.87	182.55	−60.46	92.51	194.02	−92.03
D2	183.00	136.37	42.27	133.80	176.31	−38.54	100.92	193.51	−83.95
D3	206.70	133.49	66.37	156.98	174.32	−15.72	110.25	199.83	−81.22
D4	190.85	144.62	41.92	141.42	184.89	−39.42	104.02	204.81	−91.38
A2	44.49	210.88	−150.94	31.76	223.64	−173.96	16.56	235.86	−198.82
A3	23.71	227.01	−184.32	15.05	236.90	−201.13	5.09	247.62	−219.88
R1	72.54	195.96	−111.89	48.76	217.00	−152.53	37.32	223.75	−169.01
R2	88.58	190.00	−91.95	63.61	211.83	−134.38	43.89	224.07	−163.36
R3	94.42	189.33	−86.05	69.31	211.30	−128.73	46.19	225.71	−162.75

Table 10
The FTIR bonds selected for analysis of volatiles components of CRMB binders.

Wavenumber (cm^{-1})	3013	953	2363	2180	3056	2936
Volatiles components	CH_4	C_2H_4	CO_2	CO	-C–H (aromatic)	-C–H (aliphatic)

between the products and reactants of degradation CRMB is smaller than that of partial-swelling and full-swelling CRMB binders.Table 10..

Regarding the Gibbs free energy ΔG, all CRMB binders dispaly a positive value, which illustrates that it is not possible for the pyrolysis reaction to proceed spontaneously, and the additional energy should be supplemented to promote the thermal reaction of CRMB. It is demonstrated that the ΔG value of degradation CRMB binder is higher than that of the swelling sample, indicating the former presents larger total internal energy. The positive and negative ΔS parameters during CRMB binder pyrolysis reaction are obtained, and most of the ΔS values are negative. It suggests that the reaction system is close to thermal equilibrium. Moreover, the degradation degree of CRMB would decrease the ΔS value and improve the orderliness of reaction products.

4.4. FTIR analysis

To analyze the pyrolysis products of the CRMB binder, the FTIR spectrometer was utilized to detect the gaseous components during the pyrolysis process. Fig. 9 depicts the FTIR curves at different temperatures for the partial-swelling CRMB binder with a heating rate of 100 °C /min. The specific peak at 2359 cm^{-1} exists in all FTIR curves, which refers to the release of carbon dioxide CO_2. The peak intensity of CO_2 increases first and the maximum amount of CO_2 is released when the pyrolysis temperature reaches 390 °C. Afterward, the intensity of CO_2 decreases gradually. When the temperature increases to 435 °C, new peaks at 3113, 3016, and 2957 cm^{-1} are detected, which represents the -C–H (aromatic), CH_4 (methane), and -C–H (aliphatic), respectively. These new peaks are more dominant when the temperature reaches 480 and 525 °C. Two new characteristic peaks of the carbon monoxide CO are observed when the temperature is 480 °C, which are located at 2174 and 2110 cm^{-1}. Meanwhile, these new characteristic peaks at 1305, 1182, 950, 730, and 672 cm^{-1} are more significant when the temperatures are 480 and 525 °C, which represents the functional groups of CH_4, ester C-O-C, ethylene C_2H_4, methylene –CH_2-, and benzene. The alkynyl functional group at 3316 cm^{-1} is also observed.

Similarly, the FTIR results of pyrolysis products for the full-swelling and full-degradation CRMB binders at different temperatures are illustrated in Fig. 10. The full-swelling and full-degradation CRMB binders exhibit similar characteristic peaks at different temperatures except for 525 °C. When the pyrolysis temperature is 525 °C, the full-swelling CRMB binder presents the stronger peaks regarding the functional groups of -C–H (aromatic), CH_4, -C–H (aliphatic), and C_2H_4 than the full-degradation sample. It indicates that more gaseous products are released during the pyrolysis process of swelling CRMB binder than degradation ones. Besides, the intensity of CO_2 characteristic peak of degradation CRMB is larger than that of swelling CRMB binder dramatically. During the pyrolysis process, the full-swelling CRMB binder releases more hydrocarbons than full-degradation CRMB, while the latter releases more CO_2. Hence, the degradation degree promotes the oxidation reaction of CRMB molecules and reduces the yield of gaseous hydrocarbons.

Fig. 11 depicts the evolution of different gaseous products as a function of temperature during the thermal pyrolysis process of the partial-swelling, full-swelling, and full-degradation CRMB binders. Fig. 11 (a) and (b) display the variety of CH_4 and C_2H_4, which is mainly resulted from the chemical breaking and rearrangement of side chains in aliphatic hydrocarbons. There was only one apparent absorption peak in CH_4 and C_2H_4 curves, which are located at 400–550 °C. Moreover, the maximum intensity of CH_4 and C_2H_4 is observed at approximately 450–480 °C, which is influenced by the swelling and degradation degree of the CRMB binder. The CH_4 and C_2H_4 peak temperature of full-degradation CRMB is lower than that of partial- and full-swelling CRMB samples, which implies that the generation of CH_4 and C_2H_4 from full-degradation is earlier. Meanwhile, the CH_4 and C_2H_4 intensity of CRMB is in the following order: full-swelling > partial swelling > full-degradation. It implies that the degradation process reduces the yield of gaseous hydrocarbons distinctly, while the swelling degree shows the opposite influence.

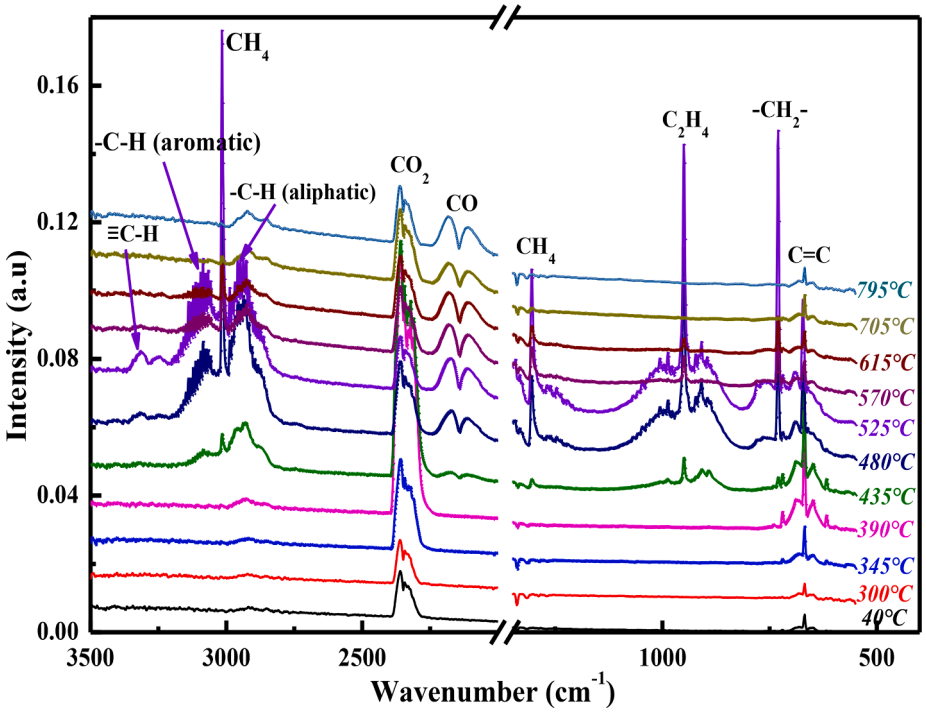

Fig. 9. The FTIR spectrum of partial-swelling CRMB binder at different temperatures.

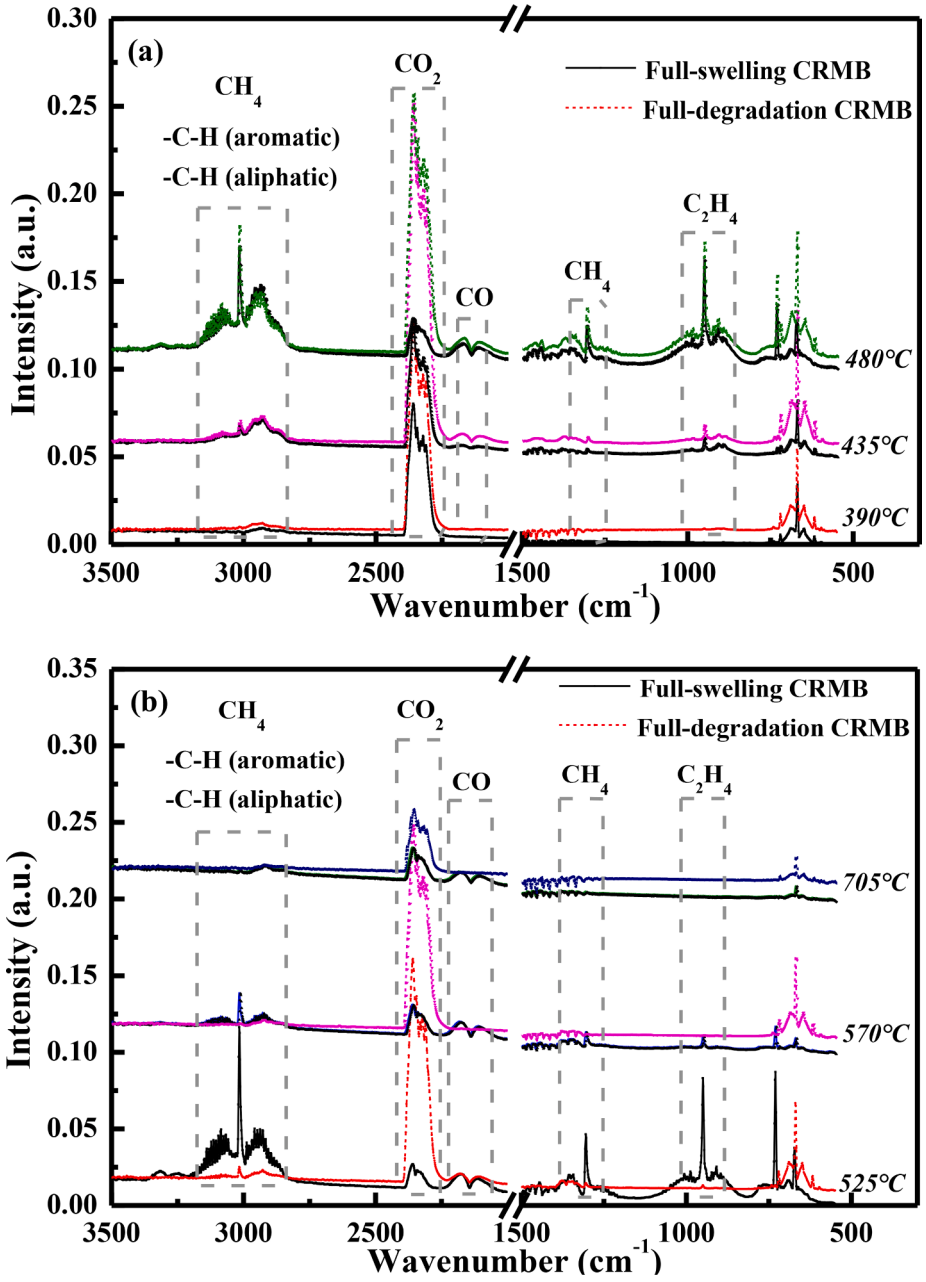

Fig. 10. The FTIR spectrum of full-swelling and full-degradation CRMB binders at different pyrolysis temperatures of (a) 390–480 °C and (b) 525–705 °C.

In addition, the evolution of the stretching vibration of -C–H (aromatic) and -C–H (aliphatic) of CRMB binders along with the pyrolysis temperature is displayed in Fig. 11 (e) and (f), respectively. The generation mechanism of the -C–H is similar to the aforementioned CH_4 and C_2H_4. As the temperature rises, the intensity of -C–H in aromatic and aliphatic hydrocarbons increases first and then decreases gradually. Compared with partial- and full-swelling samples, the full-degradation CRMB binder exhibits a lower peak temperature and -C–H intensity, which is consistent with the results of CH_4 and C_2H_4. Interestingly, the intensity of -C–H is lower than CH_4 and C_2H_4, illustrating that the cleavage products are mainly hydrocarbons with short chains. Moreover, the -C–H (aromatic) concentration of all CRMB binders is lower than the -C–H (aliphatic) content. During the thermal pyrolysis of CRMB, more aliphatic hydrocarbons than aromatic products are released.

The greenhouse and harmful gas CO_2 and CO concentrations during the pyrolysis procedure of CRMB binders are illustrated in Fig. 11 (c) and (d). It is worth mentioning that the CO_2 is generated at a low pyrolysis temperature of 200–400 °C, and other gaseous products have not appeared yet. Besides, the CO_2 peak temperature of the CRMB binder is close to 400 °C and lower than that of other pyrolysis products. Compared with swelling CRMB binder, the CO_2 concentration is higher. Hence, the degradation degree accelerates the release of CO_2 during the pyrolysis process of the CRMB binder. Additionally, the CO peak temperature of the CRMB binder is similar to other hydrocarbons. The full-swelling CRMB binder releases CO with the highest concentration, while the CO concentration from the full-degradation CRMB binder is the lowest. In summary, the degradation process accelerates the full oxidation of molecules in CRMB during the pyrolysis process, but the high swelling degree leads to the increased release of toxic gas CO.

5. Conclusions and recommendations

In this study, the swelling-degradation and thermal pyrolysis

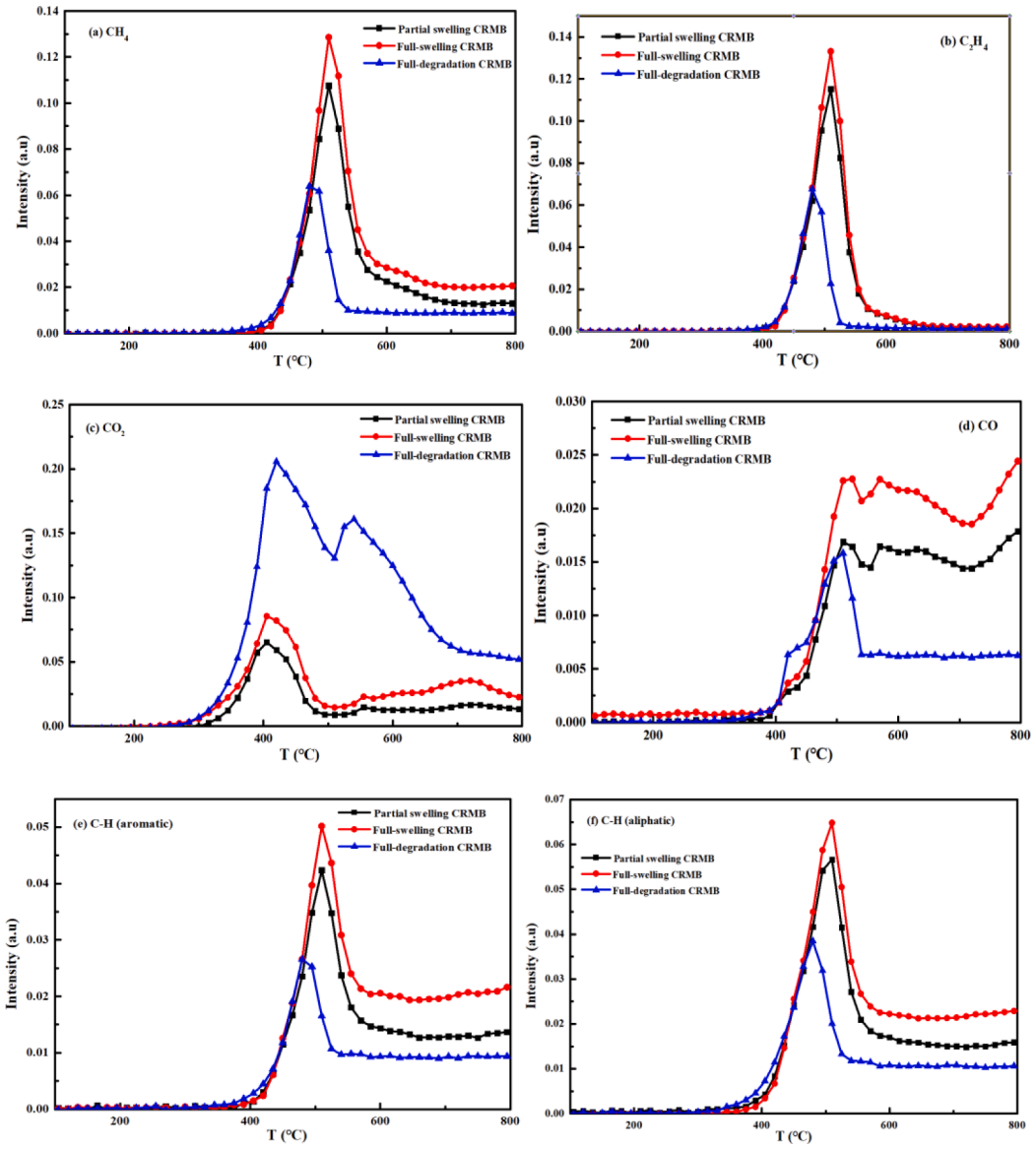

Fig. 11. The volatile components as a function of temperature. (a) CH_4; (b) C_2H_4; (c) CO_2; (d) CO; (e) C–H (Aromatic); (f) C–H (Aliphatic).

behaviors of CRMB binders were estimated by rheology and TG-FTIR. It is of interest to know how those aspects change with a more viscous bitumen, which could introduce some significant variations into the present future work indication. The main conclusions are as follows.

(1) During the 160℃-swelling process, the 135℃-viscosity of the CRMB binder increased until reaching an equilibrium value of 10.5 Pa·s at 8 h. Meanwhile, during the 200℃-degradation procedure, the viscosity increased to a maximum value of 20.58 Pa·s at 7.5 h, followed by a significant reduction to a stable value of 11.09 Pa·s. Moreover, the high temperatures accelerate the swelling rate and shorten the equilibrium time of the CRMB binder.

(2) As the swelling time prolongs, the G* and R% of CRMB both enhanced, while the δ and J_{nr} decreased. The degradation process exhibited the opposite influence. The high swelling and low degradation degree were beneficial to improve the rutting and deformation resistance.

(3) Compared to swelling CRMB, the degradation sample showed a lower thermodynamic parameter of T_S, R_e, Ea, A, ΔH, and ΔS, but higher DTG_{max} and ΔG. The degradation process accelerated the pyrolysis rate of the CRMB binder.

(4) The main gaseous products of the CRMB binder during the pyrolysis process were CH_4, C_2H_4, CO_2, CO, and other aliphatic/aromatic hydrocarbons. Besides, the released products from the full-degradation CRMB binder were less than partial- and full-swelling CRMB, except for the CO_2. The degradation process promoted the full oxidization of molecules in the CRMB binder and hindered the release of toxic gas CO.

This paper focused on the rheological properties variation of crumb rubber modified bitumen during the swelling and degradation process, and more chemical characteristics and interaction reaction mechanism should be further investigated. At the same time, the effects of swelling-degradation degree on the low-temperature and fatigue cracking behaviors of CRMB binder need to be studied. Finally, it is interesting and meaningful to explore the compositions of the gases produced during the swelling-degradation process of CRMB binder for future work.

CRediT authorship contribution statement

Shisong Ren: Methodology, Investigation, Formal analysis, Writing – original draft, Writing – review & editing. **Xueyan Liu:** Supervision, Writing – review & editing. **Peng Lin:** Methodology, Supervision, Writing – review & editing. **Sandra Erkens:** Supervision, Writing – review & editing.

Declaration of Competing Interest

The authors declare that they have no known competing financial interests or personal relationships that could have appeared to influence the work reported in this paper.

Acknowledgments

The first author greatly thanks to the funding support from the China Scholarship Council (CSC., No. 201906450025).

References

[1] V.H. Nanjegowda, K.P. Biligiri, Recyclability of rubber in asphalt roadway systems: A review of applied research and advancement in technology, Resour. Conserv. Recycl. 155 (2020), 104655, https://doi.org/10.1016/j.resconrec.2019.104655.
[2] L.G. Picado-Santos, S.D. Capitao, J.M.C. Neves, Crumb rubber asphalt mixtures: a literature review, Constr. Build. Mater. 247 (2020), 118577, https://doi.org/10.1016/j.conbuildmat.2020.118577.
[3] Q. Wang, N. Wang, M. Tseng, Y. Huang, N. Li, Waste tire recycling assessment: road application potential and carbon emissions reduction analysis of crumb rubber modified asphalt in China, J. Cleaner Prod. 249 (2020), 119411, https://doi.org/10.1016/j.jclepro.2019.119411.
[4] X. Ding, T. Ma, W. Zhang, D. Zhang, Experimental study of stable crumb rubber asphalt and asphalt mixture, Constr. Build. Mater. 157 (2017) 975–981, https://doi.org/10.1016/j.conbuildmat.2017.09.164.
[5] Z. Leng, R.K. Padhan, A. Sreeram, Production of a sustainable paving material through chemical recycling of waste PET into crumb rubber modified asphalt, J. Cleaner Prod. 180 (2018) 682–688, https://doi.org/10.1016/j.jclepro.2018.01.171.
[6] Z. Dong, T. Zhou, H. Luan, R.C. Williams, P. Wang, Z. Leng, Composite modification mechanism of blended bio-asphalt combining styrene-butadiene-styrene with crumb rubber: a sustainable and environmental-friendly solution for wastes, J. Cleaner Prod. 214 (2019) 593–605, https://doi.org/10.1016/j.jclepro.2019.01.004.
[7] W. Gui, L. Liang, L. Wang, X. Gao, F. Zhang, Performance evaluation of warm-mixed crumb rubber modified asphalt based on rheological characteristics, Constr. Build. Mater. 285 (2021), 122881, https://doi.org/10.1016/j.conbuildmat.2021.122881.
[8] X. Yang, Z. You, M.R.M. Hasan, A. Diab, H. Shao, S. Chen, D. Ge, Environmental and mechanical performance of crumb rubber modified warm mix asphalt using Evotherm, J. Cleaner Prod. 159 (2017) 346–358, https://doi.org/10.1016/j.jclepro.2017.04.168.
[9] M. Zhao, R. Dong, Reaction mechanism and rheological properties of waste cooking oil pre-desulfurized crumb tire rubber/SBS composite modified asphalt, Constr. Build. Mater. 274 (2021), 122083, https://doi.org/10.1016/j.conbuildmat.2020.122083.
[10] J. Ma, M. Hu, D. Sun, T. Lu, G. Sun, S. Ling, L. Xu, Understanding the role of waste cooking oil residue during the preparation of rubber asphalt, Resour. Conserv. Recycl. 167 (2021), 105235, https://doi.org/10.1016/j.resconrec.2020.105235.
[11] T. Zhou, S.F. Kabir, L. Cao, E.H. Fini, Effects of ultraviolet exposure on physicochemical and mechanical properties of bio-modified rubberized bitumen: Sustainability promotion and resource conservation, Resour. Conserv. Recycl. 171 (2021), 105626, https://doi.org/10.1016/j.resconrec.2021.105626.
[12] S.F. Kabir, R. Zheng, A.G. Delgado, E.H. Fini, Use of microbially desulfurized rubber to produce sustainable rubberized bitumen, Resour. Conserv. Recycl. 164 (2021), 105144, https://doi.org/10.1016/j.resconrec.2020.105144.
[13] X. Yang, A. Shen, B. Li, H. Wu, Z. Lyu, H. Wang, Z. Lyu, Effect of microwave-activated crumb rubber on reaction mechanism, rheological properties, thermal stability, and released volatiles of asphalt binder, J. Cleaner Prod. 248 (2020), 119230, https://doi.org/10.1016/j.jclepro.2019.119230.
[14] D. Li, Z. Leng, F. Zhou, H. Yu, Effects of rubber absorption on the aging resistance of hot and warm asphalt rubber binders prepared with waste tire rubber, J. Cleaner Prod. 303 (2021), 127082, https://doi.org/10.1016/j.jclepro.2021.127082.
[15] M. Liang, X. Xin, W. Fan, S. Ren, J. Shi, H. Luo, Thermo-stability and aging performance of modified asphalt with crumb rubber activated by microwave and TOR, Mater. Des. 127 (2017) 84–96, https://doi.org/10.1016/j.matdes.2017.04.060.
[16] I. Gawel, R. Stepkowski, F. Czachowski, Molecular interactions between rubber and asphalt, Ind. Eng. Chem. Res. 46 (9) (2006) 3044–3049, https://doi.org/10.1021/ie050905r.
[17] J. Li, Z. Chen, F. Xiao, S.N. Amirkhanian, Surface activation of scrap tire crumb rubber to improve compatibility of rubberized asphalt, Resour. Conserv. Recycl. 169 (2021), 105518, https://doi.org/10.1016/j.resconrec.2021.105518.
[18] D. Dong, X. Huang, X. Li, L. Zhang, Swelling process of rubber in asphalt and its effect on the structure and properties of rubber and asphalt, Constr. Build. Mater. 29 (2012) 316–322, https://doi.org/10.1016/j.conbuildmat.2011.10.021.
[19] H. Wang, X. Liu, P. Apostolidis, S. Erkens, T. Scarpas, Numerical investigation of rubber swelling in bitumen, Constr. Build. Mater. 214 (2019) 506–515, https://doi.org/10.1016/j.conbuildmat.2019.04.144.
[20] W. Huang, P. Lin, N. Tang, J. Hu, F. Xiao, Effect of crumb rubber degradation on components distribution and rheological properties of terminal blend rubberized asphalt binder, Constr. Build. Mater. 151 (2017) 897–906, https://doi.org/10.1016/j.conbuildmat.2017.03.229.
[21] F. Xu, B. Wang, D. Yang, J. Hao, Y. Qiao, Y. Tian, Thermal degradation of typical plastics under high heating rate conditions by TG-FTIR: Pyrolysis behaviors and kinetic analysis, Energy Convers. Manage. 171 (2018) 1106–1115, https://doi.org/10.1016/j.enconman.2018.06.047.
[22] X. Ming, F. Xu, Y. Jiang, P. Zong, B. Wang, J. Li, Y. Qiao, Y. Tian, Thermal degradation of food waste by TG-FTIR and Py-GC/MS: Pyrolysis behaviors, products, kinetic and thermodynamic analysis, J. Cleaner Prod. 244 (2020), 118713, https://doi.org/10.1016/j.jclepro.2019.118713.
[23] J. Hao, W. Feng, Y. Qiao, Y. Tian, J. Zhang, Y. Che, Thermal cracking behaviors and products distribution of oil sand bitumen by TG-FTIR and Py-GC/TOF-MS, Energy Convers. Manage. 151 (2017) 227–239, https://doi.org/10.1016/j.enconman.2017.08.083.
[24] J. Hao, Y. Che, Y. Tian, D. Li, J. Zhang, Y. Qiao, Thermal cracking characteristics and kinetics of oil sand bitumen and its SARA fractions by TG-FTIR, Energy Fuels 31 (2017) 1295–1309, https://doi.org/10.1021/acs.energyfuels.6b02598.
[25] X. Wei, H. Zhang, Q. Yang, E. Yao, Y. Zhang, H. Zou, Studying the mechanisms of natural rubber pyrolysis gas generation using RMD simulations and TG-FTIR experiments, Energy Convers. Manage. 189 (2019) 143–152, https://doi.org/10.1016/j.enconman.2019.03.069.
[26] F. Xu, B. Wang, D. Yang, X. Ming, Y. Jiang, J. Hao, Y. Qiao, Y. Tian, TG-FTIR and Py-GC/MS study on pyrolysis mechanism and products distribution of waste bicycle tire, Energy Convers. Manage. 175 (2018) 288–297, https://doi.org/10.1016/j.enconman.2018.09.013.
[27] J. Zhao, X. Huang, T. Xu, Combustion mechanism of asphalt binder with TG-MS technique based on components separation, Constr. Build. Mater. 80 (2015) 125–131, https://doi.org/10.1016/j.conbuildmat.2014.11.056.
[28] W. Xia, T. Xu, H. Wang, Thermal behaviors and harmful volatile constituents released from asphalt components at high temperature, J. Hazard. Mater. 2019 (373) (2019) 741–752, https://doi.org/10.1016/j.jhazmat.2019.04.004.
[29] W. Xia, T. Xu, H. Wang, Y. Pan, Combustion kinetics of asphalt binder components and the release processes of gaseous products, Combust. Flame 206 (2019) 322–333, https://doi.org/10.1016/j.combustflame.2019.05.009.
[30] Xia W., Xu T. (2020). Thermal characteristics, kinetics models, and volatile constituents during the energy conversion of bituminous SARA fractions in air. ACS OMEGA, 2020, 5, 33, 20831-20841. https://doi.org/10.1021/acsomega.0c02023.
[31] M. Elkashef, R.C. Williams, E. Cochran, Thermal stability and evolved gas analysis of rejuvenated reclaimed asphalt pavement (RAP) bitumen using thermogravimetric analysis-Fourier transform infrared (TG-FTIR), J. Therm. Anal. Calorim. 131 (2018) 865–871, https://doi.org/10.1007/s10973-017-6674-9.
[32] AASHTO T316-13. Standard method of test for viscosity determination of asphalt binder using rotational viscometer.
[33] AASHTO T320. Standard specification for performance-graded asphalt binder.
[34] Aashto tp70., Standard method of test for multiple stress creep recovery (MSCR) test of asphalt binder using a Dynamic Shear Rheometer (DSR), American Association of State Highway and Transportation Officials, Washington (DC), 2009.